Title	A first principles investigation of Bi2O3-modified TiO2 for visible light activated photocatalysis: the role of TiO2 crystal form and the Bi3+ stereochemical lone pair
Authors	Lucid, Aoife K.;Iwaszuk, Anna;Nolan, Michael
Publication date	2014-09
Original Citation	LUCID, A., IWASZUK, A. & NOLAN, M. 2014. A first principles investigation of Bi2O3-modified TiO2 for visible light Activated photocatalysis: The role of TiO2 crystal form and the Bi3+ stereochemical lone pair. Materials Science in Semiconductor Processing, 25, 59-67. DOI: http://dx.doi.org/10.1016/j.mssp.2014.01.005
Type of publication	Article (peer-reviewed)
Link to publisher's version	http://www.sciencedirect.com/science/article/pii/S1369800114000080 - 10.1016/j.mssp.2014.01.005
Rights	© 2014 Elsevier Inc. All rights reserved. NOTICE: this is the author's version of a work that was accepted for publication in Materials Science In Semiconductor Processing. Changes resulting from the publishing process, such as peer review, editing, corrections, structural formatting, and other quality control mechanisms may not be reflected in this document. Changes may have been made to this work since it was submitted for publication. A definitive version was subsequently published in Materials Science In Semiconductor Processing [Volume 25, September 2014, Pages 59–67] http://dx.doi.org/10.1016/j.mssp.2014.01.005
Download date	2024-09-18 14:27:31
Item downloaded from	https://hdl.handle.net/10468/1645

University College Cork, Ireland
Coláiste na hOllscoile Corcaigh

A First Principles Investigation of Bi_2O_3-Modified TiO_2 for Visible Light Activated Photocatalysis: the Role of TiO_2 Crystal Form and the Bi^{3+} Stereochemical Lone Pair

Aoife Lucid, Anna Iwaszuk, and Michael Nolan*

Tyndall National Institute, University College Cork, Lee Maltings, Dyke Parade, Cork, Ireland

michael.nolan@tyndall.ie

Highlights

- First principles simulations of TiO_2 rutile (110), anatase (101) and anatase (001) surfaces modified with Bi_2O_3 nanoclusters as potential visible light active photocatalyst
- A reduction in the energy gap over TiO_2 is predicted for Bi_2O_3-modified rutile (110).
- Enhanced charge separation after photoexcitation is predicted, with holes localised on Bi_2O_3 and electrons on TiO_2.
- There is little change in the energy gap for Bi_2O_3-modified anatase and electrons and holes reside on anatase.
- The effect of the Bi^{3+} lone pair is much reduced compared to Sn^{2+}

Abstract.

Modification of TiO_2 with metal oxide nanoclusters is a novel strategy for the design of new photocatalysts with visible light activity. This paper presents a first principles density functional theory (DFT) analysis of the effect of modifying TiO_2 rutile (110) and anatase (101) and (001) surfaces with Bi_2O_3 nanoclusters on the band gap and the nature of the photoexcited state. We show that band gap modifications over unmodified TiO_2 depend on the crystal form: modifying rutile (110) results in new Bi_2O_3 derived states that shift the valence band upwards. On anatase surfaces, there is little effect due to modification with Bi_2O_3 nanoclusters, but an enhanced UV activity would be expected. Analysis of electron and hole localisation in a model photoexcited state shows enhanced charge separation in Bi_2O_3-modified rutile (110) but not in Bi_2O_3-modified anatase. The effect of the Bi^{3+} lone-pair on the properties of Bi_2O_3-modified TiO_2 contrasts with SnO-modified TiO_2, consistent with the weaker lone pair in Bi_2O_3 compared with SnO.

Graphical Abstract

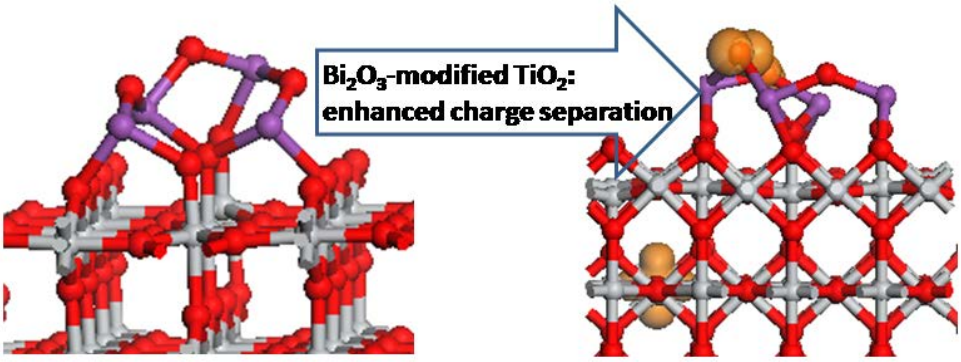

The effect of modifying TiO_2 with Bi_2O_3 nanoclusters depends on the crystal form of TiO_2

Keywords: Photocatalysis, TiO_2, Bi_2O_3, Lone Pair, Density functional theory, Energy gap

1. Introduction

With the problems of diminishing fossil fuel supply, global warming and CO_2 emissions, as well as widespread environmental pollution, solar energy driven photocatalysis for fuel production or pollution remediation is of great interest and TiO_2 based photocatalysts receive a significant level of attention [1-6]. As a photocatalyst, TiO_2 is a very good candidate, with low cost, good availability, stability and non-toxicity. However the main drawback is that the band gap of TiO_2 means it absorbs in the UV region of the electromagnetic spectrum, which makes up around only 5 % of the visible solar spectrum. The ability to modify TiO_2 for visible light absorption brings with it the possibility for solar driven photocatalysis in areas such as water splitting, environmental remediation and bacterial removal.

There have been many attempts to reduce the band gap of TiO_2 to enable visible light absorption and photocatalytic activity [7-]. The primary approach in band gap engineering has been either metal doping at Ti sites [7 – 13] or non-metal doping at O sites [14 – 20] of TiO_2. More recently, so-called “co-doping” of a metal and non-metal at the Ti and O sites is receiving some attention [21,22]. It is usually concluded that the visible light absorption originates from the formation of new dopant-derived defect states formed in the energy gap of TiO_2. These states are supposed to facilitate electronic transitions from filled dopant states to empty conduction band states of TiO_2 or from filled valence band of TiO_2 to empty dopant states and these transitions have energies in the visible region.

However, the formation of these localised defect states will, unfortunately, reduce photocatalytic efficiency by acting as recombination centres, trapping electrons or holes. This was shown recently by Hermann for Cr-doped TiO_2 [XX]. Simultaneous metal-non metal co-doping of TiO_2 is proposed as an alternative so long as the dopants charge compensate each other and remove the localised defect states [21], and has been demonstrated experimentally for, e.g. C/Mo co-doped TiO_2 [22].

A different approach to designing effective photocatalysts is to fabricate heterostructures composed from rutile-anatase composites or modification with another metal oxide [23-31]. The formation of the interface between the two phases in composites or TiO_2 and the modifier can change the electronic structure to introduce visible light absorption and enhance charge carrier separation [23-31]. Iron oxide nanoclusters have been deposited onto anatase TiO_2 using atomic layer deposition of iron oxide by Libera et al. [23] and by chemisorption-calcination-cycling (CCC) deposition of transition metal oxide nanoclusters by Tada and co-workers [24, 25, 29, 32]. These experiments have reported band gap reduction, predominantly from an upwards shift in the valence band edge as determined by X-ray photoelectron spectra and a reduction in electron/hole recombination from photoluminescence spectroscopy [23, 25, 29]. Enhanced visible and UV photocatalytic activity for oxidation of organic molecules over unmodified TiO_2 has also been demonstrated [23 - 25, 29, 32]. Accompanying theoretical work from our group using density functional theory (DFT) studies has shown that TiO_2 modified with TiO_2 [30], FeOx [27], Ga_2O_3 [31] and NiO [32] nanoclusters will lead to a band gap reduction over unmodified TiO_2 and we have discussed the enhanced charge carrier separation and electron and hole polaronic localisation.

We have also discovered that the stereochemical lone pair in SnO can give rise to a notable difference between SnO and SnO_2 modified TiO_2 [29, 33], which was also found for SnO/SnO_2 modified $ZnGa_2O_4$ [34], although in the latter paper, this difference was not discussed. Briefly, the lone pair present in SnO [35] results in new SnO-derived states being introduced above the original VB edge of TiO_2, which reduces the energy gap over unmodified TiO_2, while for SnO_2 the lack of the lone pair means there is little if any band gap change [29, 33].

In light of this interesting effect due to the stereochemical lone pair, we present in this paper a first principles analysis of TiO_2 rutile (110) and anatase (101) and (001) surfaces modified with Bi_2O_3 nanoclusters, which contain Bi^{3+} species that have a stereochemically active lone pair [36], which is weaker than in SnO. The presence of Bi^{3+} in materials such as $BiVO_4$ and Bi_2WO_6 is considered to be important for their photocatalytic activity in that it is important in determining the nature of the valence band of the material [36, 37].

We show from our first principles simulations that the effect of Bi_2O_3 modifications to rutile and anatase depends on the crystal form of TiO_2: modifying rutile (110) with Bi_2O_3 nanoclusters results in a reduction of the energy gap compared with unmodified rutile, giving enhanced visible light absorption and charge separation. However, modifying anatase TiO_2 gives little change to the band gap of TiO_2 and will not enhance charge separation. Thus both the modifier and the crystal form of TiO_2 can be used to tune the activity of modified TiO_2 by inducing enhanced visible or UV light absorption.

2. Computational Methods

To model TiO_2 rutile (110) surface, we use a three dimensional periodic slab model within the VASP code [38]. The valence electrons were described by a plane wave basis set and the cut-off for the kinetic energy is 396 eV. The number of valence electrons is 4 for Ti, 5 for Bi and 6 for O. A recent study highlighted that the Ti semi-core 3s and 3p states can have an effect on the computed properties of bulk TiO_2 [39], we have also repeated selected calculations with a larger 12 valence electron PAW potential on the Ti atoms in each surface; the results of this comparison are discussed in section 3 and given in detail in the Supporting Information.

The exchange-correlation functional is the Perdew-Wang 91 [40] approximation. We use

a Monkhorst-Pack (2×1×1) k-point sampling grid in all calculations. In describing Ti *3d* states and in particular for structures that can contain reduced Ti^{3+} species as a result of transferring electrons to previously (formally) empty Ti 3*d* states, the well known DFT+U approach [41,42] is applied and we use a value of U = 4.5 eV on the Ti 3*d* states that has been used in our previous work on this topic [30, 32, 33]. For Bi, the electronic states for both oxidation states are consistently described by DFT so no +U correction is applied here. To examine any effects due to applying DFT+U on the relative positions of the TiO_2 and Bi_2O_3 energy states and consequent modifications to the energy gap of TiO_2, we have also repeated some calculations using DFT without the +U correction and the details are presented in the supporting information. While hybrid DFT could be used instead of DFT+U, the size of our systems precludes the use of hybrid DFT within a plane wave basis set.

The rutile (110) surface (figure 1(a)) is terminated by two-fold coordinated bridging O atoms and the Ti atoms in the surface are 5-fold and 6-fold coordinated. A (2x4) surface supercell expansion is employed. For anatase, the (101) and unreconstructed (001) surface are shown in figures 1(b) and (c); we have successfully used the unreconstructed (001) surface in our other studies [32]. Both anatase surfaces are characterised by two-fold coordinated oxygen atoms terminating the surface layer and the outermost Ti atoms are 5-fold coordinated. A (4x2) surface supercell expansion of anatase (101) and (001) is employed. These surface supercells allow adsorption of isolated nanoclusters and the vacuum gap in all cases is 12 Å. The surface models are stoichiometric with no defects and no adsorbed hydroxyl species, both of which are well known defects in TiO_2 surfaces, but this model suffices for understanding the basic properties of modified TiO_2. The convergence criteria for the electronic and ionic relaxations are 0.0001 eV and 0.02 eV/ Å. For the consistency in the calculation we also applied the same supercell and

technical parameters for the bare TiO_2 surface and free clusters.

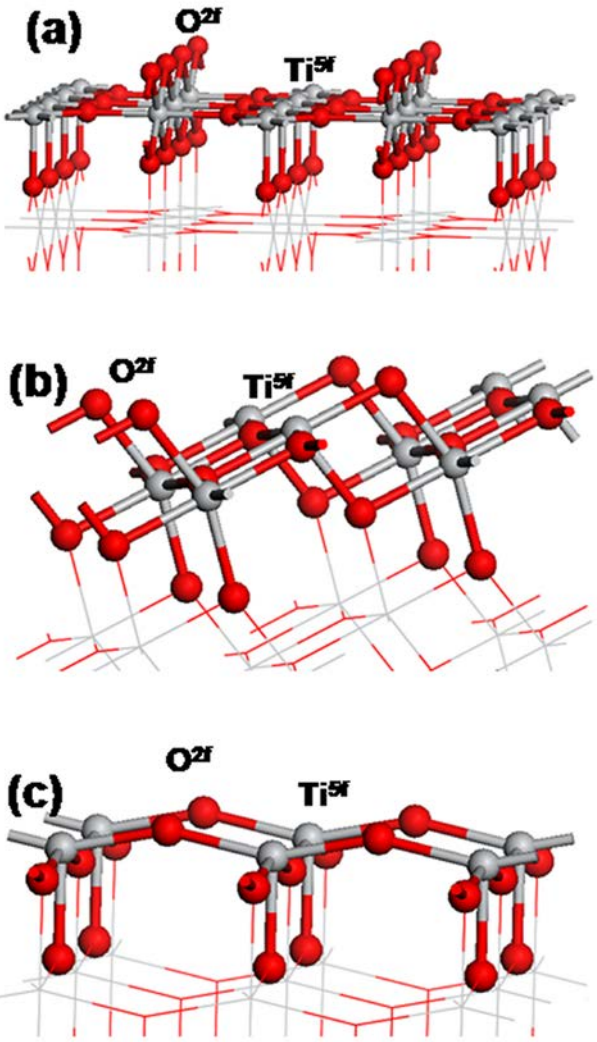

Figure 1: Atomic structures of the bare (a) rutile (110), (b) anatase (101) and (c) unreconstructed anatase (001) surfaces used in this work. Two-fold coordinated oxygen and five-fold coordinated Ti are indicated as O^{2f} and Ti^{5f}.

The clusters are positioned on the TiO_2 surfaces and the adsorption energy is computed from:

$$E\text{ads} = E((Bi_2O_3)\text{-}TiO_2) - \{ E(Bi_2O_3) + E(TiO_2) \} \qquad (1)$$

Where $E((Bi_2O_3)\text{-}TiO_2)$ is the total energy of the Bi_2O_3 nanocluster supported on the anatase surface and $E(Bi_2O_3)$ and $E(TiO_2)$ are the total energies of the free Bi_2O_3 cluster and the unmodified anatase surface. A negative adsorption energy indicates that cluster adsorption is stable.

To examine how surface modification of TiO_2 affects electron and hole localisation over unmodified TiO_2 and to examine the energetics of this process, we study a model of photoexcited Bi_2O_3-modified rutile (110) and anatase (101). The photoexcited system is modelled as the lowest energy DFT+U solution for an imposed triplet electronic state. This model generates an excited electron and a hole by construction in which the excited electron is found in the conduction band and the hole is found in the valence band. We and others have previously discussed in detail this approach in refs. [31, 33, 43 - 45]. The following energies are calculated:

The ground state energy of the system, denoted $E^{singlet}$

A single point energy of a triplet state, at the ground state geometry, denoted $E^{unrelaxed}$

An ionic relaxation of the triplet electronic state, $E^{relaxed}$.

From these energies, we extract

(1) The singlet-triplet vertical unrelaxed excitation energy: $E^{vertical} = E^{singlet} – E^{unrelaxed}$

(2) The singlet-triplet excitation energy: $E^{S\text{-}T} = E^{singlet} – E^{relaxed}$. This energy should not be compared to the optical gap, nor is it the excitation energy that would be obtained from a time dependent DFT simulation of the lowest energy excited state, but it can be compared between modifications of TiO_2 to assess the effect of the modifier on the band gap shift [31, 33].

(3) The electron and hole trapping energy: $E^{relax} = E^{relaxed} – E^{unrelaxed}$. E^{relax} is the energy gained when the electron and hole are trapped at their Ti and O sites (forming polarons) accompanied by structural relaxation around the polarons.

The resulting energies will be underestimated due to well known deficiencies in DFT, but are useful in making comparisons between similar systems, e.g. refs. [31, 32, 44].

3. Results

3.1 Adsorption Energies and Structures of TiO_2 Rutile and Anatase Modified with Bi_2O_3 Nanoclusters

Figure 2 presents the relaxed atomic structures together with adsorption energies for representative structures of the model rutile (110) surface modified with Bi_2O_3, Bi_4O_6 and Bi_6O_9 nanoclusters. All nanoclusters adsorb strongly at the rutile (110) surface, showing large negative adsorption energies of -5.76 eV for Bi_2O_3 and -5.18 eV for the other nanoclusters and create new interfacial metal-oxygen bonds. The magnitude of these energies indicates that the nanoclusters will be anchored at the surface and will not aggregate into large particles or films [46].

A comparison between the 4 valence and 12 valence electron potentials for Ti, as well as between the DFT+U correction on Ti 3d states and no DFT+U correction indicates that the effect of the potential or the DFT+U correction is not significant, in that the strong adsorption of Bi_2O_3 nanoclusters at rutile (110) is not affected.

The Bi_2O_3 nanocluster bonds to the rutile (110) surface with three new bonds between oxygen from the nanocluster and Ti from the surface, with O-Ti distances of 1.91, 1.93 and 2.10 Å. Bi atoms in the nanocluster bind to two bridging oxygen from the surface, with O-Bi distances of 2.24 and 2.26 Å, which are consistent with Bi-O distances in Bi_2O_3. Within the

Bi_2O_3 nanocluster, the Bi-O distances are 2.02 and 2.21 Å for one Bi atom and 2.05 and 2.23 Å for the second Bi atom.

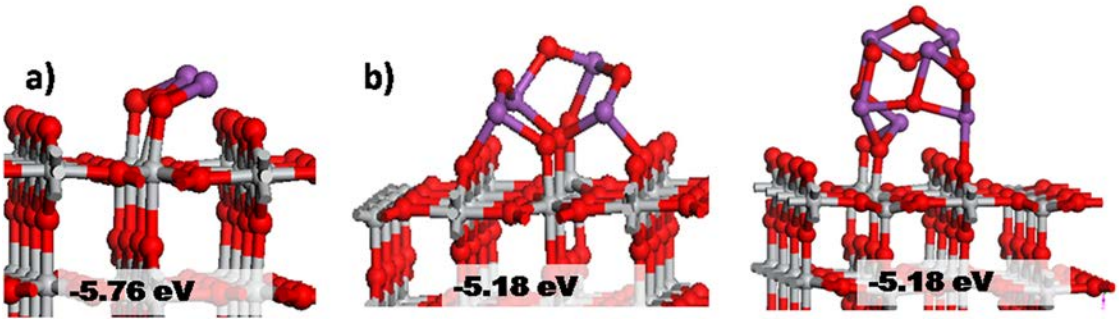

Figure 1. Relaxed adsorption structures with adsorption energies given in eV for (a) Bi_2O_3, (b) Bi_4O_6 and (c) Bi_6O_9 nanoclusters supported on rutile (110) TiO_2. Ti atoms are grey spheres, oxygen is red and Bi atoms are purple and this colour scheme is used throughout the paper.

The adsorption of the Bi_4O_6 nanocluster results in five new bonds between the nanocluster and the surface. There are two bonds from Bi atoms to bridging surface oxygen, which have Bi-O distances of 2.17 Å. There are three new bonds between oxygen in the nanocluster and the 5-fold coordinated Ti surface atoms, with Ti-O distances in the range of 1.83 Å to 2.05 Å. In the largest Bi_2O_3 nanocluster, there is a new Bi-O bond to bridging oxygen in the surface, with a distance of 2.37 Å, while oxygen from the nanocluster bind to Ti atoms in the surface, with Ti-O distances of 1.94 and 1.86 Å. Bi-O distances in the nanocluster range from 2.09 to 2.28 Å, with low coordinated oxygen in the nanocluster displaying the longest Bi-O distances.

Comparing with Bi-O bond distances in bulk Bi_2O_3, which lie in the range of 2.19 Å to 2.59 Å [47], the Bi-O distances in the nanoclusters are generally shorter, arising from the lower coordination of Bi in the nanoclusters compared to bulk. The surface Ti atoms that bind to the

nanocluster are pulled out of the surface layer by the interaction with oxygen and this displacement is around 0.45 Å, lengthening the subsurface Ti-O distances involving these Ti atoms to around 2.20 Å.

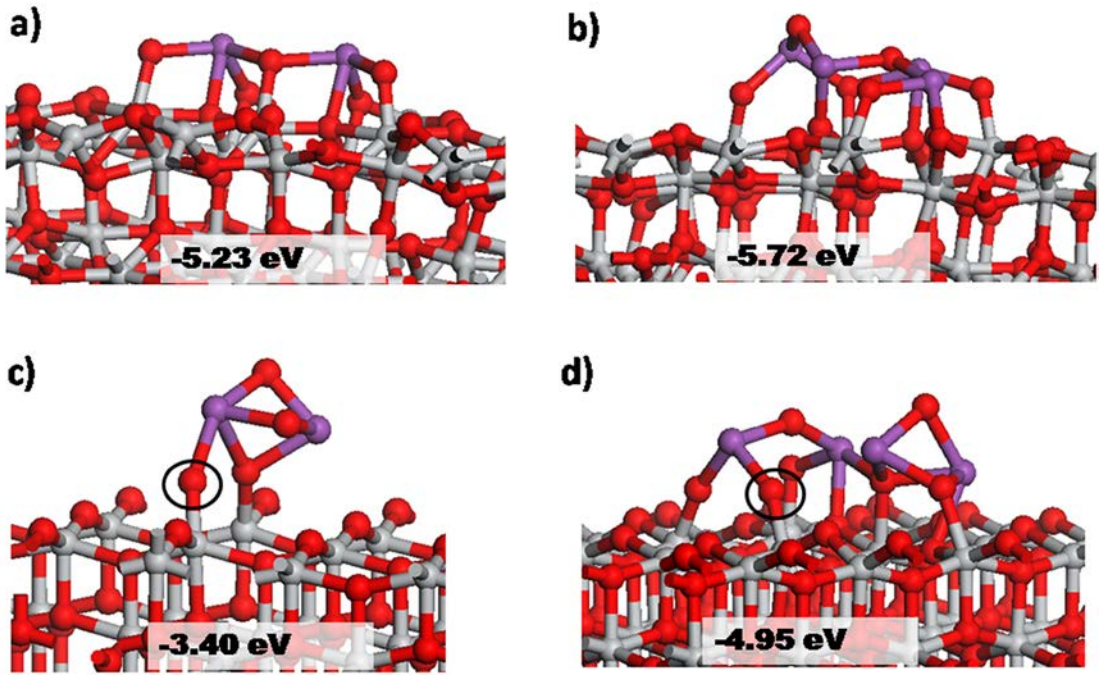

Figure 3. Relaxed adsorption structures with adsorption energies given in eV for (a) Bi_2O_3 modified anatase (101) (b) Bi_4O_6 modified anatase (101), (c) Bi_2O_3 modified anatase (001) and (d) Bi_4O_6 modified anatase (001). The colour scheme is the same as figure 2 and the rings around oxygen atoms in (c) and (d) indicate oxygen from the anatase (001) surface that are pulled out of the surface layer upon interaction with the Bi_2O_3 nanoclusters.

Figure 3 shows the atomic structure of Bi_2O_3 and Bi_4O_6 nanoclusters adsorbed on the anatase (101) and (001) surfaces. Both Bi_2O_3 nanoclusters adsorb strongly at the two anatase surface, making a number of new nanocluster-surface interfacial bonds. The adsorption energies at both anatase surfaces are negative, again indicating a strong interfacial interaction between the nanocluster and the surface. The adsorption energies at anatase (101) are similar

to those are rutile (110) and both are notably larger than at anatase (001). The origin of this difference will be discussed in the following paragraphs. We further find that the strong adsorption of Bi_2O_3 nanoclusters at anatase (001) is not affected by using the 12 valence electron potential on Ti or a lack of +U correction on the Ti 3d states (see supporting information).

For Bi_2O_3 adsorbed at the anatase (101) surface, there is one new bond between each oxygen in the nanocluster and a 5-fold coordinated surface Ti atom, with O-Ti distances of 1.88, 1.90 and 2.04 Å. Each Bi in the nanocluster binds to two surface terminating oxygen atoms, with Bi-O distances of 2.22 and 2.27 Å, typical of Bi-O distances. Within the nanocluster, the Bi-O distances are 2.13 – 2.27 Å, similar to Bi_2O_3 adsorbed at rutile (110).

At anatase (001), the Bi_2O_3 nanocluster adsorbs in an interesting fashion. There is a new O-Ti bond involving oxygen from the nanocluster, with an O-Ti distance of 1.92 Å. When the nanocluster adsorbs at anatase (001), a surface oxygen atom is pulled out of the terminating layer of oxygen atoms to make a new bond to a Bi atom in the nanocluster, with a Bi-O distance of 2.19 Å; the removal of an oxygen from the anatase (001) surface upon adsorption of metal oxide nanoclusters has been seen in our previous work on SnO_2 [29] and SnO [33] modified anatase (001). There is an energy cost associated with displacing this oxygen off its lattice site and since the overall adsorption energy is a balance between energy gained when making new interfacial bonds and the energy cost to distort the surface, this energy cost contributes to the smaller nanocluster adsorption energy found at anatase (001) compared to rutile (110) or anatase (101). Within the Bi_2O_3 nanocluster, the Bi-O distances are 2.06 – 2.33 Å.

For Bi_4O_6 adsorption at both surfaces, we observe again that at anatase (001) an oxygen from the surface layer of anatase (001) is pulled out of the surface to make a new Bi-O bond, with a Bi-O distance of 2.06 Å. This Bi is only 3-fold coordinated, with short Bi-O distances of

2.07 and 2.11 Å to oxygen in the nanocluster. Two further nanocluster Bi atoms make new bonds to anatase (001), with Bi-O distances of 2.16 and 2.35 Å. There are three new O-Ti bonds between nanocluster oxygen and Ti in the surface, with distances of 1.86, 2.08 and 2.10 Å. At the (101) surface, four new Bi-O bonds to the surface are formed, with Bi-O distances of 2.14, 2.24, 2.14 and 2.17 Å, which are typical of the Bi-O distances found in the interface between the nanocluster and the surface. There are also four new bonds between nanocluster oxygen and surface Ti, with distances of 1.87, 1.89, 2.0, 2.01 and 2.06 Å; the shortest O-Ti distances are for the 2-coordinated oxygen atoms in the nanocluster.

3.2 Electronic Structure and Band Gap Changes in TiO_2 Rutile and Anatase Surfaces Modified with Bi_2O_3 Nanoclusters.

Figures 4 to 6 present the electronic density of states (PEDOS) projected onto Bi 6*s* and O 2*p* states of the Bi_2O_3 nanoclusters and Ti3 *d* and O 2*p* states of TiO_2 modified with Bi_2O_3 nanoclusters. The PEDOS are shown for rutile (110) in figure 4, anatase (101) in figure 5, and anatase (001) in figure 6. The PEDOS plots allow us to investigate any band gap changes due to modifying TiO_2 with Bi_2O_3 nanoclusters.

The PEDOS plots show that the effect of the Bi_2O_3 modification of rutile (110) depends on the nanocluster size; this corresponds to a change in nanocluster loading in experimental work on surface modification of TiO_2 [29]. The modification of rutile (110) with the Bi_2O_3 nanocluster makes no change in the energy gap of TiO_2. The Bi 6s and Bi_2O_3-derived O 2p states lie below the VB edge of TiO_2 and will therefore not modify the energy gap. Similarly, empty Bi_2O_3 nanocluster states lie above the rutile (110) CB edge. Thus, the VB-CB gap in unmodified and Bi_2O_3-modified TiO_2 is 2.1 eV in both cases.

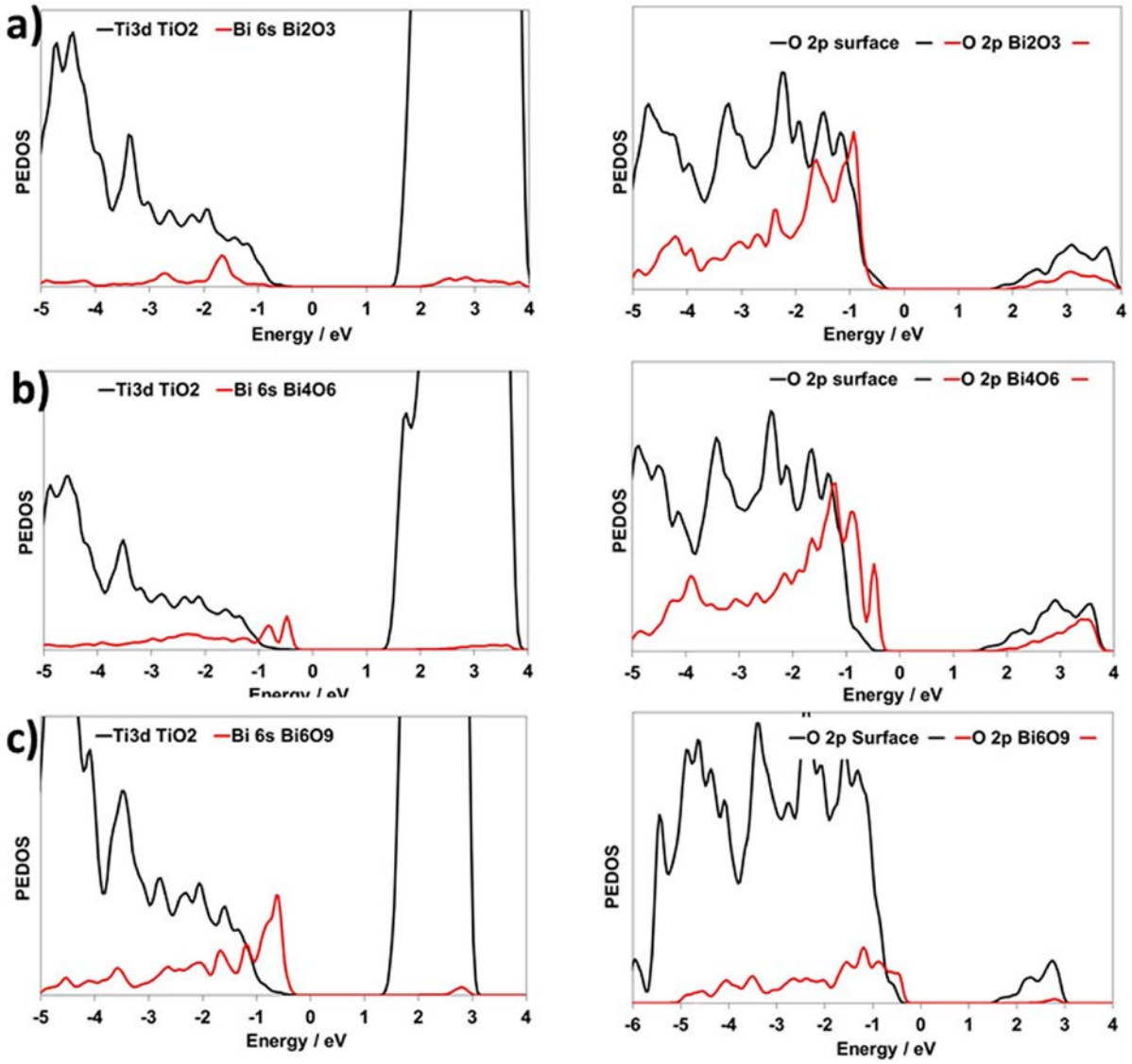

Figure 4: Electronic density of states projected (PEDOS) onto Bi 6s and Ti 3d (left panels) and O2p (from the nanocluster and the TiO_2 surface, right panels) states for (a) Bi_2O_3, (b) Bi_4O_6 and (c) Bi_6O_9 nanoclusters supported on TiO_2 rutile (110) surface. The zero of energy is the Fermi level.

However when we examine the PEDOS for the larger Bi_4O_6 and Bi_6O_9 nanoclusters, we find in both cases, the modification of rutile (110) introduces new electronic states derived from Bi_2O_3 into the band gap of rutile TiO_2. These states are derived from the Bi6s-O2p

interaction, that is the lone pair, in the Bi_2O_3 nanoclusters. These nanocluster derived states lie above the valence band edge of the rutile (110) surface, and as a consequence the original band gap of TiO_2 will be reduced by the upwards shift in the energy of the valence band edge. The CB edge is unmodified by the surface modification. This size of the shift in the energy gap is 0.3 eV for the Bi_4O_6 nanocluster and 0.1 eV for the Bi_6O_9 nanocluster and for the former nanocluster, may be large enough to induce some visible light absorption upon photoexcitation. We will return to this point in a subsequent section.

When we compare the effect of the Ti potential and the +U correction on the PEDOS of Bi_2O_3-rutile (110), see supporting information, we find that there is no change to the general picture discussed above. Irrespective of the choice of Ti potential or DFT+U correction, there is no change to the VB or CB edges of rutile (110). This provides confidence in our chosen computational set-up for this problem.

In figures 5 and 6 we display the PEDOS for anatase (101) and (001) surfaces modified with Bi_2O_3 and Bi_4O_6 nanoclusters. From the PEDOS a striking difference with modified rutile (110) is immediately apparent. The PEDOS for Bi_4O_6-modified anatase (101) and (001) does not show a change in the nature of the valence band edge – the Bi_2O_3 derived electronic states lie below the CB edge of both anatase surfaces, with the VB to CB energy gap unchanged over unmodified anatase (101) and (001), at 2.3 eV.

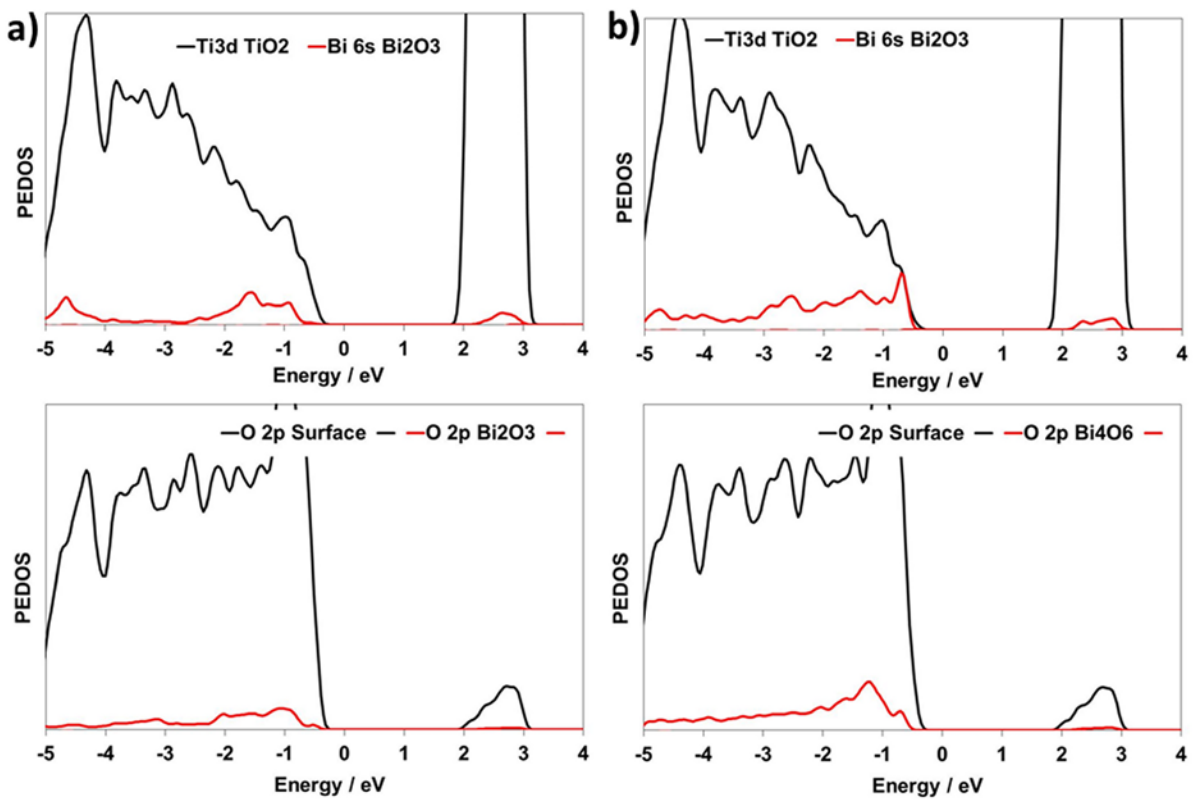

Figure 5: Electronic density of states projected (PEDOS) onto Bi 6s and Ti 3d (top panels) and O2p (from the nanocluster and the TiO_2 surface, bottom panel) states. (a) Bi_2O_3 and (b) Bi_4O_6 nanocluster modified anatase (101) surface. The zero of energy is the Fermi level.

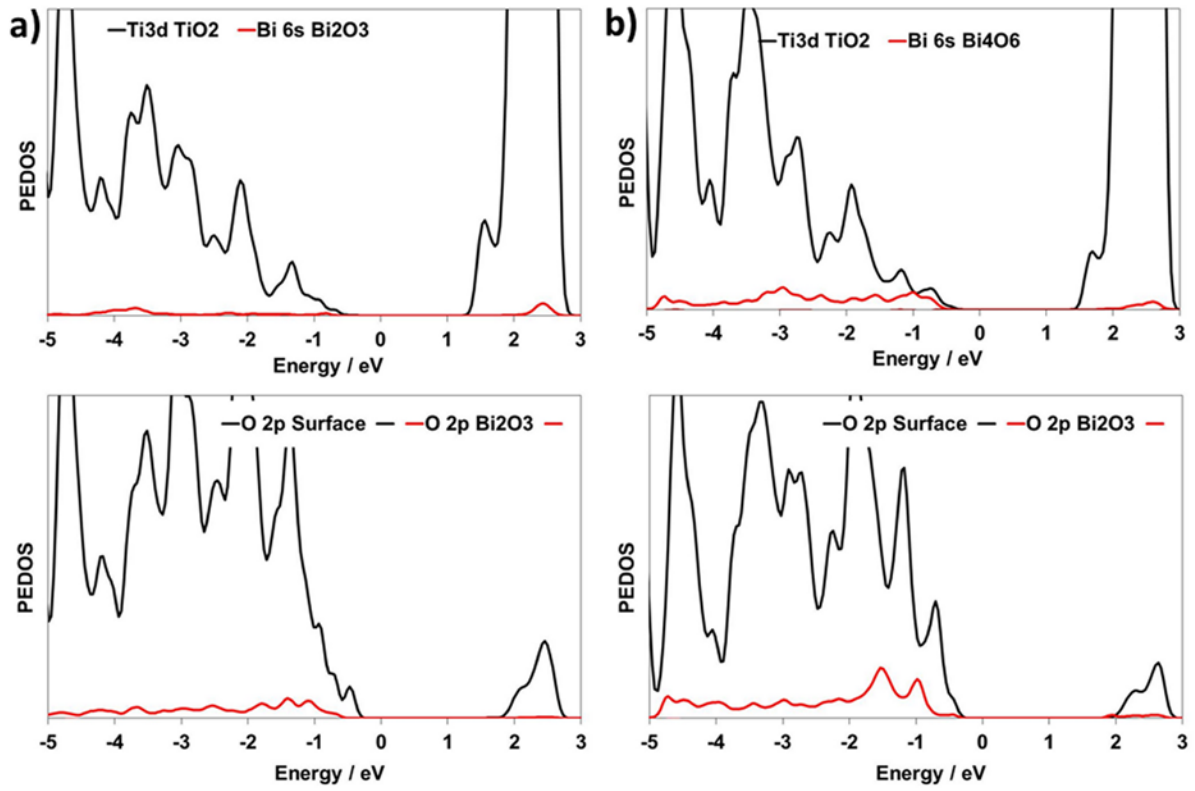

Figure 6: Electronic density of states projected (PEDOS) onto Bi 6s and Ti 3d (top panels) and O2p (from the nanocluster and the TiO_2 surface, bottom panel) states. (a) Bi_2O_3 and (b) Bi_4O_6 nanocluster modified anatase (001) surface. The zero of energy is the Fermi level.

The final point from the PEDOS analysis is the composition of the VB and CB in modified TiO_2 which will give an indication of the expected sites for electron and hole localisation which is important for charge separation and photocatalytic activity. Taking, Bi_4O_6 modified rutile and anatase surfaces as an example, in Bi_4O_6-rutile, the valence band edge is derived primarily from Bi 6s and O 2p states in the nanocluster and the conduction band edge is derived from Ti 3d states of the surface. This composition of the VB and CB edges will result in hole localisation on the Bi_4O_6 nanocluster and electron localisation on the rutile (110) surface which will enhance electron/hole separation after photoexcitation.

On the other hand, for Bi_4O_6-modified anatase surfaces a different fate is predicted for the photoexcited electrons and holes: both electrons and hole will be localised onto the rutile (110) surface, which will lead to no improvement in charge carrier separation upon excitation with light of energy around the band gap energy. However, comparing to other oxide-modified anatase structures where no visible light activity is induced, e.g. SnO_2-modified anatase [23, 29], the presence of unoccupied Bi_4O_6 states above the TiO_2 CB means that with sufficiently energetic UV radiation, an electron can be promoted to empty Bi_4O_6 nanocluster states that would facilitate charge separation in this case. The excited electron could reduce O_2 to superoxide, which would be reactive in decomposition of organic molecules.

We have previously shown that FeO_x [27], Ga_2O_3 [31] and NiO [32] nanocluster modification of rutile TiO_2 can also produce a similar band gap narrowing to Bi_4O_6/Bi_6O_9-modified rutile, due to a widening of the valence band arising from an upwards shift in the VB edge as a result of the introduction of electronic states from the oxide nanocluster above the TiO_2 VB edge. All these oxides form strong interfacial bonds to rutile, which is a key factor in determining the effect of the oxide nanocluster modification on the electronic structure. There have been fewer such studies on modified anatase, but we have found that the larger energy gap for anatase compared to rutile can result in no change in the energy gap for modified anatase, e.g. for SnO_2 [29], which is also found in the present work.

4. Electron and Hole Localisation in a Model of the Photoexcited State

To study charge separation and localisation in Bi_2O_3 modified TiO_2, we use a model of the photoexcited state, as discussed in section 2. For unmodified TiO_2 refs. 31, 43 and 44 have examined electron and hole localisation in bulk anatase and the (101) surface [43], in rutile

(110) [31, 44] and in modified rutile (110) [31]. Hybrid DFT or DFT+U are required in order to describe the localised charge carriers and their polaronic nature.

Figure 7 shows the computed excess spin density for two examples: (1) the Bi_4O_6 nanocluster supported on rutile (110) and (2) the Bi_4O_6 nanocluster supported on anatase (001). The spin density is used to determine the positions of the electron and hole and their localisation in the photoexcited state.

In the photoexcited state of Bi_4O_6-modified rutile, the electron is localised on a surface Ti site which reduced to Ti^{3+} species and this is further confirmed by a calculated Bader charge [48] of 1.67 electrons and a computed spin magnetisation of 0.9 electrons. This localisation is accompanied by a strong elongation in the Ti-O distances of 0.1 Å, typical of the elongation of Ti-O distances around a Ti^{3+} polaron. The electronic hole is localised on a 2-fold coordinated oxygen atom in the Bi_4O_6 nanocluster, with a computed Bader charge of 6.7 electrons and a spin magnetisation of 0.73 electrons. The Bi-O distances around this oxygen are elongated to 2.29 and 2.37 Å, consistent with a localised oxygen hole polaron. There is a slight spreading of the hole onto a second O atom from the cluster, which has a small change in the Bader charge from 7.30 electrons for O^{2-} to 7.09 and a small spin magnetisation 0.14 electrons. Nonetheless, it is clear that the valence band hole localises onto a low coordinated oxygen site in the Bi_4O_6 nanocluster.

We see that there is no Bi^{3+} contribution to the electronic hole despite the presence of Bi 6s electronic states around the valence band edge. This would be consistent with the weaker lone pair effect in Bi_2O_3, when compared to SnO, which shows a stronger lone pair effect [35].

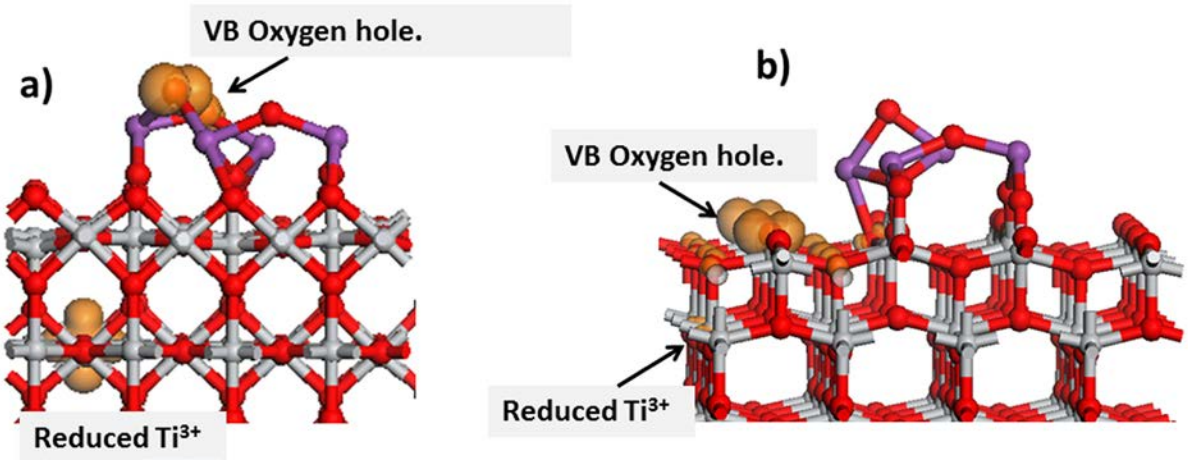

Figure 7. Computed excess spin density isosurfaces for the photoexcited state of the Bi_4O_6 cluster supported on (a)) the rutile (110) surface and (b) the anatase (001) surface. The spin density isosurfaces enclose spin densities up to 0.02 electrons / $Å^3$.

Figure 7(b) shows the spin density for Bi_4O_6-modified anatase (001). Here we see a difference compared to Bi_4O_6 modified rutile. There is no localisation of the excited electron or hole onto the nanocluster, which is consistent with the simple analysis of the DOS presented above, which indicates that the photoexcited hole would be found on oxygen from anatase and the photoexcited electron would be found on Ti from anatase. The spin density shows that the hole is spread over two surface oxygen atoms (similar to hole localisation on bare anatase (001) [33]), while the electron is spread over subsurface Ti atoms, each of which is partially reduced.

The singlet-triplet excitation energy for Bi_4O_6-modified rutile (110) is 1.20 eV, which is smaller than the same energy for unmodified rutile (110), which is 1.69 eV [31]. This is consistent with the finding from the DOS analysis and indicate that this modification of rutile will be beneficial in inducing absorption of longer wavelength light. The relaxation energy is

0.83 eV, which is consistent with localisation of the hole on the nanocluster and subsequent relaxation of the structure in response to the formation of the localised oxygen hole [31, 33].

For Bi_4O_6-modified anatase, the computed singlet-triplet excitation energy is 1.89 eV, which is a small reduction over the vertical singlet-triplet energy of 2.01 eV, consistent with the electron and hole being found on the surface, where large relaxations are not possible. These findings support the analysis of the density of states that modifying rutile with Bi_2O_3 nanoclusters can reduce the energy gap, but that modifying anatase will not reduce the energy gap.

5. Conclusions

We have presented the results of a first principles DFT analysis of modification of TiO_2 rutile (110) and anatase (101) and (001) with nanoclusters of bismuth oxide. We investigated the changes in the band gap of the modified material over pure TiO_2 rutile (110) together with the potential of enhanced electron/hole separation upon photoexcitation.

Our DFT results reveal that modification of rutile (110) with Bi_2O_3 nanoclusters can induce a reduction of the original band gap of unmodified rutile (110), by an upwards shift in the valence band edge and this is dominated by Bi 6s and O 2p states from the Bi_2O_3 nanocluster. The exact effect depends on the size, or loading, of the nanocluster on the surface. This will reduce the band gap but the reduction may not be sufficiently large to induce activity in the visible region upon photoexcitation. Enhanced activity in the UV region will be likely. In contrast, modifying anatase surfaces will Bi_2O_3 nanoclusters will lead to no change in the band gap, with no modifications to the valence or conduction band.

A model of the photoexcited states shows that the Bi_2O_3-rutile structure will enhance the separation of hole and electrons upon photoexcitation by localising the hole and electron on the nanocluster and the surface, respectively. A comparison with SnO modified TiO_2 rutile (110) [33] shows that the lone pair effect is weaker in Bi_2O_3 than in SnO nanoclusters which is similar to the findings of bulk SnO and Bi_2O_3 [35]. For Bi_2O_3 modified anatase, the electron and hole are localised onto the anatase surface.

These results show that the change in the key properties for photocatalytic activity in TiO_2 can be modified by choice of TiO_2 crystal form and the size (or loading) of the modifying oxide nanocluster.

Acknowledgements

We acknowledge support from Science Foundation Ireland (SFI) through the Starting Investigator Research Grant Program, project "EMOIN", grant number SFI 09/SIRG/I1620. Access to computing resources at Tyndall is funded by SFI and by the SFI and Higher Education Authority funded Irish Centre for High End Computing and by the European Union FP7 Research Infrastructures Program PRACE, through the DECI-8 program, contracts RI-261557 and RI-283493. We acknowledge support from the European Union through the COST Action CM1104 "Reducible Oxide Chemistry, Structure and Functions". Prof. Hiroaki Tada is thanked for useful discussions and his support of this work.

References

1. H. Choi, M. G. Antoniou, M. Pelaez, A. Delacruz, J. Shoemaker and D. D. Dionysiou, Environ. Sci. Technol. 41, 7530 (2007)

2. H. Yu, H. Irie, Y. Shimodaira, Y. Hosogi, Y. Kuroda, M. Miyauchi and K. Hashimoto, J. Phys. Chem. C, 114, 16481 (2010)

3. A. Fujishima, X. Zhang and D. A. Tryk, Surf. Sci. Rep. 63, 515 (2008)

4. M. Ni, M. Leung, D. Leung and K. Sumathy, Renew. Sust. Energ. Rev. 11, 401 (2007)

5. J. Zhao, C. Chen and W. Ma, Top. Catal. 35, 269 (2005)

6. J. Nowotny, Energy Environ. Sci. 2, 556 (2008)

7. Y. Cui, H. H. Du and L. S. Wen, J. Mat. Sci. and Tech. 24, 675 (2008)

8. X. L. Nie, S. P. Zhou, G. Maeng and K. Sohlberg, Int. J. Photoenergy article 294042 (2009).

9. A. Iwaszuk and M. Nolan, J. Phys. Chem. C, 115, 12995 (2011)

10. J. M. Herrmann, New. J. Chem. 36, 883 (2012)

11. L. Bian, M. X. Song, T. L. Zhou, X. Y. Zhao and Q. Q. Dai, J. Rare Earths 27, 461 (2009)

12. T. Ikeda, T. Nomoto, K. Eda, Y. Mizutani, H. Kato, A. Kudo and H. Onishi, J. Phys. Chem. C 112, 1167 (2008)

13. K. Yang, Y. Dai and B. Huang, ChemPhysChem 10, 2327 (2009)

14. R. Asahi, T. Morikawa, T. Ohwaki, K. Aoki and Y. Taga, Science 293, 269 (2001)

15. K. Yang, Y. Dai and B. Huang, J. Phys. Chem. C 111, 12086 (2007)

16. C. Di Valentin, E. Finazzi, G. Pacchioni, A. Selloni, S. Livarghi, M. C. Paganini and E. Giamello, Chem. Phys, 339, 44 (2007)

17. R. Long and N. J. English, J. Phys. Chem. C 114, 11984 (2010)

18. J. W. Zheng, A. Bhattcahrayya, P. Wu, Z. Chen, J. Highfield, Z. L. Dong and R. Xu, J. Phys. Chem. C 114, 7063 (2010)

19. S. U. M. Khan, M. Al-Shahry, W. B. Ingler Jr., Science 297, 2243 (2002)

20. K. Yang, Y. Dai, B. Huang and M-H Whangbo, J. Phys. Chem. C 113, 2624 (2009)

21. Y. Q. Gai, J. B. Li, S. S. Li, J. B. Xia and S. H. Wei, 102, 036402 (2009)

22. J. Zhang, C. X. Pan, P. F. Fang, J. H. Wie and R. Xiong, ACS Appl. Mater. Interfaces, 2, 1173 (2010)

23. J. A. Libera, J. W. Elam, N. F. Sather, T. M. Rajh and N. M. Dimitrijevic, Chem. Mater, 22, 409 (2010)

24. Q. Jin, M. Fujishima and H. Tada, J. Phys. Chem C 115, 6478 (2011)

25. M. Fujishima, Q. Jin, H. Yamamoto, H. Tada and M. Nolan, Phys. Chem. Chem. Phys., 14, 705 (2012)

26. N. Murakami, T. Chiyoya, T. Tsubota and T. Ohno, Appl. Catal. A 348, 148 (2008)

27. M. Nolan, Phys. Chem. Chem. Phys., 13, 18194 (2011)

28. H. Yu, H. Irie, Y. Shimodaira, Y. Hosogi, Y. Kuroda, M. Miyauchi and K. Hashimoto, J. Phys. Chem. C 114, 16481 (2010)

29. A. Iwaszuk, M. Nolan, Q. Jin, M. Fujishima and H. Tada, J. Phys. Chem. C, 116, 12621 (2012)

30. A. Iwaszuk and M. Nolan, Phys. Chem. Chem. Phys. 13, 4963 (2011)

31. M. Nolan, ACS Appl. Mater. Interfaces, 4, 5863 (2012)

32. A. Iwaszuk, M. Nolan, Q. Jin, M. Fujishima and H. Tada, Journal of Physical Chemistry C, 117, 2709 (2013)

33. A. Iwaszuk and M. Nolan, J. Mat. Chem. A, 1, 6670 (2013)

34. V. B. R. Boppana and R. F. Lobo, ACS Catal. 1, 923 (2011)

35. A. Walsh, D. J. Payne, R. G. Egdell and G. W. Watson, Chemical Society Reviews 40, 4455 (2011)

36. A. Walsh, Y. Yan, M. N. Huda, M. M. Al-Jassim and S. H. Wei, Chem. Mat, 21, 547 (2009)

37. C. Zhang and Y. Zhu, Chem. Mat., 17, 3537 (2005)

38. G. Kresse and J. Hafner, Phys Rev. B 49, 14251 (1994)

39. N. A. Deskins, Chem. Phys. Lett., 75, 471 (2009)

40. J. P. Perdew, J. A. Chevary, S. H. Vosko, K. A. Jackson, M. R. Pederson, D. J. Singh and C. Fiolhais, Phys. Rev. B 46, 6671 (1993)

41. B. J. Morgan and G. W. Watson, J. Phys. Chem. C 114, 2321 (2010)

42. M. Nolan, S. Grigoleit, D. C. Sayle, S. C. Parker and G. W. Watson, Surf.Sci. 576, 217 (2005)

43. C. Di Valentin and A. Selloni, J.Phys. Chem. Lett. 2, 2223 (2011)

44. A. Jedidi, A. Markovits, C. Minot, S. Bouzriba and M. Abderraba, Langmuir, 26, 16232 (2010)

45. D. Munoz Ramo, P. V. Sushko and A. L. Shluger, Phys. Rev. B, 85, 024120 (2012)

46. A. Iwaszuk, P. A. Mulheran and M. Nolan, J. Mat. Chem. A, 1, 2515 (2013)

47. A. Walsh, G. W. Watson, D. J. Payne, R. G. Edgell, J. Guo, P-A. Glans, T. Learmonth and K. E. Smith, Phys Rev B, 73, 235104 (2006)

48. G. Henkelman, A. Arnaldsson and H. Jónsson, Computational Materials Science, 36, 354 (2006)